



Modeling Group B *Streptococcus* and Blood-Brain Barrier Interaction by Using Induced Pluripotent Stem Cell-Derived Brain Endothelial Cells

Brandon J. Kim,^a Olivia B. Bee,^a Maura A. McDonagh,^a Matthew J. Stebbins,^a Sean P. Palecek,^a Kelly S. Doran,^b Eric V. Shusta^a

Department of Chemical and Biological Engineering, University of Wisconsin, Madison, Wisconsin, USA^a;
Department of Immunology and Microbiology, University of Colorado School of Medicine, Aurora, Colorado, USA^b

ABSTRACT Bacterial meningitis is a serious infection of the central nervous system (CNS) that occurs after bacteria interact with and penetrate the blood-brain barrier (BBB). The BBB is comprised of highly specialized brain microvascular endothelial cells (BMECs) that function to separate the circulation from the CNS and act as a formidable barrier for toxins and pathogens. Certain bacteria, such as *Streptococcus agalactiae* (group B *Streptococcus* [GBS]), possess the ability to interact with and penetrate the BBB to cause meningitis. Modeling bacterial interaction with the BBB *in vitro* has been limited to primary and immortalized BMEC culture. While useful, these cells often do not retain BBB-like properties, and human primary cells have limited availability. Recently, a human induced pluripotent stem cell (iPSC)-derived BMEC model has been established that is readily renewable and retains key BBB phenotypes. Here, we sought to evaluate whether the iPSC-derived BMECs were appropriate for modeling bacterial interaction with the BBB. Using GBS as a model meningeal pathogen, we demonstrate that wild-type GBS adhered to, invaded, and activated the iPSC-derived BMECs, while GBS mutants known to have diminished BBB interaction were attenuated in the iPSC-derived model. Furthermore, bacterial infection resulted in the disruption of tight junction components ZO-1, occludin, and claudin-5. Thus, we show for the first time that the iPSC-derived BBB model can be utilized to study BBB interaction with a bacterial CNS pathogen.

IMPORTANCE Here for the first time, human iPSC-derived BMECs were used to model bacterial interaction with the BBB. Unlike models previously used to study these interactions, iPSC-derived BMECs possess robust BBB properties, such as the expression of complex tight junctions that are key components for the investigation of bacterial effects on the BBB. Here, we demonstrated that GBS interacts with the iPSC-derived BMECs and specifically disrupts these tight junctions. Thus, using this BBB model may allow researchers to uncover novel mechanisms of BBB disruption during meningitis that are inaccessible to immortalized or primary cell models that lack substantial tight junctions.

KEYWORDS blood-brain barrier, group B *Streptococcus*, stem cells

Bacterial meningitis is a serious, life-threatening infection of the central nervous system (CNS) and a major cause of death and disability worldwide, with a disproportionate number of cases involving children (1–3). While current antibiotic therapy has transformed bacterial meningitis from a uniformly fatal condition into an often-curable one, mortality remains between 5 and 10%, with permanent neurologic sequelae occurring in 5 to 40% of survivors, depending on the patient's age and the

Received 10 September 2017 **Accepted** 5 October 2017 **Published** 1 November 2017

Citation Kim BJ, Bee OB, McDonagh MA, Stebbins MJ, Palecek SP, Doran KS, Shusta EV. 2017. Modeling group B *Streptococcus* and blood-brain barrier interaction by using induced pluripotent stem cell-derived brain endothelial cells. *mSphere* 2:e00398-17. <https://doi.org/10.1128/mSphere.00398-17>.

Editor Sarah E. F. D'Orazio, University of Kentucky

Copyright © 2017 Kim et al. This is an open-access article distributed under the terms of the [Creative Commons Attribution 4.0 International license](https://creativecommons.org/licenses/by/4.0/).

Address correspondence to Kelly S. Doran, kelly.doran@ucdenver.edu, or Eric V. Shusta, eshusta@wisc.edu.

O.B.B. and M.A.M. contributed equally to this work.

pathogen (1–3). To cause meningitis, bacteria must gain access to the bloodstream and replicate to a high level, causing bacteremia (1). Following bacteremia, bacteria must then interact with and penetrate the blood-brain barrier (BBB) to gain access to the central nervous system (CNS). The specialized brain microvascular endothelial cells (BMECs) that comprise the BBB respond to these bacterial interactions with a cellular immune response and contribute to the disease progression (1–3).

Streptococcus agalactiae (group B *Streptococcus* [GBS]) is a Gram-positive, non-spore-forming bacterium that is the leading cause of neonatal meningitis and is an emerging pathogen in specific adult populations (1, 4, 5). Although advancements have been made in diagnosis and therapy, death still occurs in up to 10% of cases, with 25 to 50% of surviving infants exhibiting permanent neurological sequelae (1, 4, 5). More recently, much work has been conducted to determine bacterial virulence factors that contribute to interaction with the BBB and allow bacterial access to the CNS. Bacterial surface-expressed factors, such as lipoteichoic acid (LTA) (6), pilus components (PilA, PilB, and PilC) (7, 8), serine-rich repeat proteins (Srr) (9–11), streptococcal fibronectin binding factor (SfbA) (12), fibrinogen-binding protein (FbsA) (13), and hypervirulent GBS adhesin (HvgA) (14), have all been demonstrated to promote direct association with the BBB. Additionally, regulatory two-component signal transduction systems, such as CovR/S (15), and CiaR/H (16), have been implicated in the ability to regulate virulence factors that contribute to the pathogenesis of GBS meningitis. Studies have also been conducted to determine the BBB response to GBS. During infection, immortalized BMECs have been shown to downregulate tight junctions through the induction of host transcription factor Snail1, a known repressor of tight junction components. This response resulted in a significant loss of barrier function during infection, which was dependent on Snail1 expression (17). Previous studies have also demonstrated that GBS infection of immortalized BMECs upregulates proinflammatory chemokines and cytokines that act to orchestrate the recruitment and activation of neutrophils and enhance their survival (1, 7, 18). The recruitment of neutrophils has been linked to further BBB destruction during infection, and bacterial determinants that include CovR/S, PilA, and β -hemolysin/cytolysin contribute to this process (7, 15, 18). Together, these factors promote GBS penetration of the BBB, allowing access to the CNS and the development of meningitis.

The BBB is comprised of highly specialized BMECs that serve to separate the brain from the circulation and, along with cells of the neurovascular unit (NVU), maintain CNS homeostasis (19–21). BMECs express a spectrum of nutrient transporters and multidrug efflux transporters while also displaying intercellular tight junctions and low endocytosis rates (19–21). To study the BBB, researchers have relied on complementary *in vivo* and *in vitro* techniques. Animal models have been utilized to examine bacterial interactions with the BBB in the context of the full CNS microenvironment (6, 22–28); however, these are inherently nonhuman models and subject to interspecies differences (29). Primary cell culture of animal and human BMECs has been employed (30–33); however, after removing BMECs from the brain microenvironment, they routinely lose BBB characteristics (29, 34, 35). Immortalized human BMECs offer a facile human-based model (29, 34–36), yet many of these cell lines lack critical BBB properties, such as high transendothelial electrical resistance (TEER) and complex tight junctions (29, 34–36). Recently, induced pluripotent stem cells (iPSCs) have offered the prospect of renewable BBB models with superior barrier properties (29, 34, 37–40). The model has been used to examine drug delivery, genetic human disease, and ischemic stroke, but it has not yet been evaluated for its applicability to infectious disease (41–44). Here, we demonstrate that an iPSC-derived BMEC model can be used to examine host-pathogen interactions using the meningeal pathogen GBS. These results motivate the application of this model in infectious disease research.

RESULTS

Wild-type GBS interacts with iPSC-derived BMECs. Previous studies have shown that GBS has the ability to interact with and invade immortalized human brain

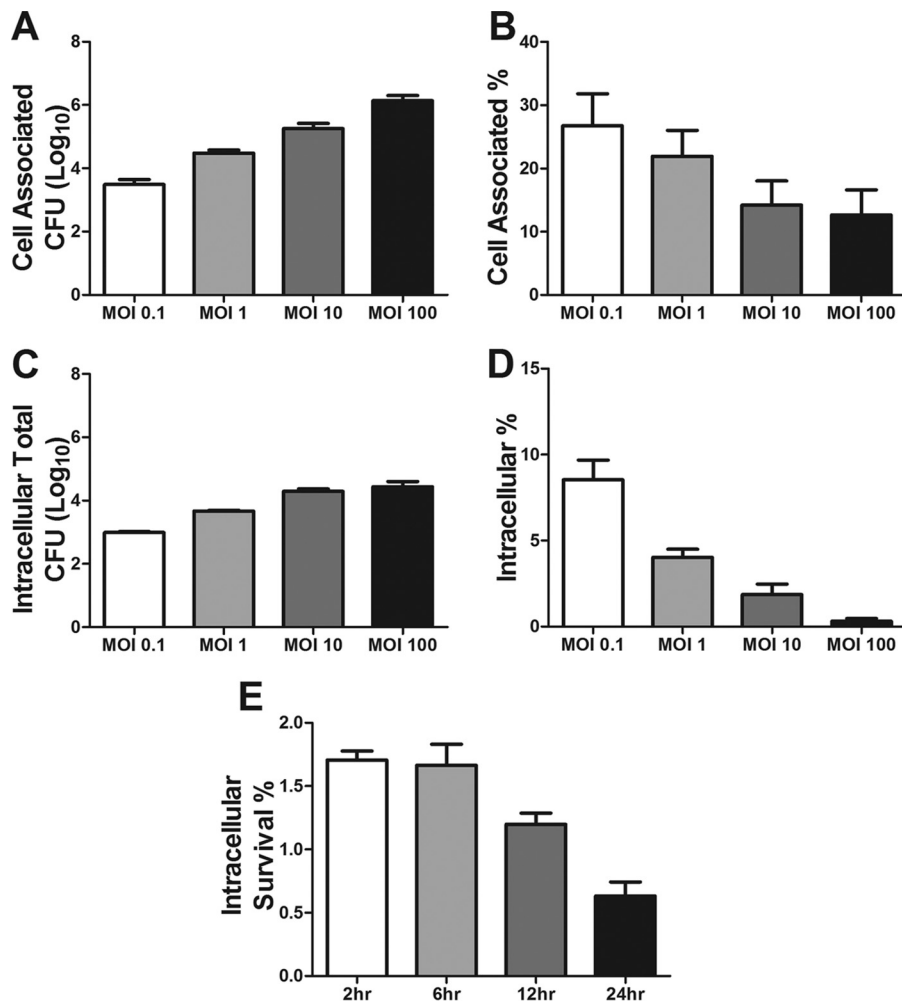


FIG 1 Interaction of group B *Streptococcus* with iPSC-derived BMECs. (A and B) Adherence of wild-type GBS to iPSC-derived BMECs over a range of MOIs, expressed as total CFU recovered (A) and percentage of initial inoculum (B). (C and D) Invasion of wild-type GBS into iPSC-derived BMECs, presented as total recovered CFU (C) and percentage of initial inoculum (D). (E) Survival of intracellular GBS, sampled from 2 to 24 h after infection of iPSC-derived BMECs at an MOI of 10, presented as the percentages of the initial inoculum. Data are presented as mean values from three independent iPSC-derived BMEC differentiations conducted in triplicate. Error bars represent SEM.

endothelial cells (hBMECs) (1, 3, 4, 14, 31). Thus, we sought to determine if iPSC-derived BMECs could be used to model these interactions. The iPSC-derived BMECs were differentiated as previously described and were shown to express the expected markers and respond to astrocyte cues (Fig. S1A to G) (29, 40). In addition, the iPSC-derived BMECs express $\beta 1$ integrin, a receptor for GBS virulence factors (Fig. S1H) (7, 12). Wild-type serotype III, hypervirulent, multilocus sequence type 17 (MLST-17) GBS strain COH1 was used to examine GBS interactions with iPSC-derived BMECs. Confluent iPSC-derived BMEC monolayers were infected with GBS to assess bacterial attachment and intracellular invasion. The numbers of total cell-associated and intracellular bacteria recovered increased proportionally with the multiplicity of infection (MOI) of the original inoculum (Fig. 1A and C). However, as the MOI increased, the percentage of adherent or intracellular GBS recovered relative to the original inoculum decreased in a stepwise fashion (Fig. 1B and D), indicating that bacterial attachment and uptake mechanisms are saturable. These results were specific to GBS, as the cell-associated and intracellular populations of the nonpathogenic bacterium *Lactococcus lactis* were significantly less than those observed for GBS (Fig. S2). To determine if GBS is able to survive intracellular uptake into iPSC-derived BMECs, we performed a modified invasion

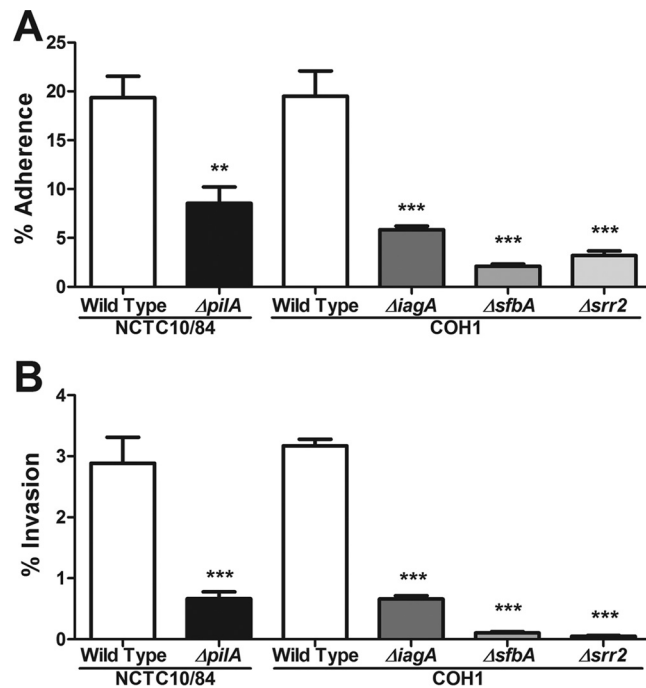


FIG 2 Contribution of GBS virulence factors to interaction with iPSC-derived BMECs. Adherence (A) and invasion (B) of wild-type GBS strains compared to those of GBS mutants lacking the virulence factors *pilA*, *iagA*, *sfbA*, and *srr2*. Data are presented as mean values from three independent iPSC-derived BMEC differentiations conducted in triplicate. Error bars represent SEM. Student's *t* test was used to determine the significance of the difference between WT NCTC10/84 and the $\Delta pilA$ mutant. ANOVA was used to determine the significance of the difference between WT COH1 and the $\Delta iagA$, $\Delta sfbA$, and $\Delta srr2$ mutants. **, $P < 0.01$; ***, $P < 0.001$.

assay in which the numbers of intracellular GBS bacteria were quantified at different time points after the addition of antibiotics to eliminate extracellular bacteria. As shown by the results in Fig. 1E, GBS persisted in iPSC-derived BMECs for up to 6 h and then exhibited a decrease in intracellular survival over time. Overall, these data demonstrate that GBS can specifically interact with iPSC-derived BMECs and are consistent with results obtained in immortalized hBMECs and other cell types (16, 31, 45, 46).

GBS virulence factors contribute to interaction with iPSC-derived BMECs. Recently, much work has been conducted to identify and characterize virulence factors that promote GBS interaction with the BBB (6–8, 11–14, 47). To determine whether several well characterized GBS virulence factors affected interactions with iPSC-derived BMECs, a cohort of mutants were examined for their ability to promote attachment and invasion of the iPSC-derived BMECs. We selected GBS factors that have been shown to be critical for BBB interaction and the pathogenesis of GBS meningitis. Specifically, we chose surface-expressed factors, including PilA (7, 8), SfbA (47), and Srr2 (9, 10), all of which contribute to GBS interaction with extracellular matrix (ECM) components acting to bridge the bacteria to host ECM receptors (1). Additionally, we analyzed the contribution of an invasion-associated gene (*iagA*) whose product acts to anchor lipoteichoic acid (LTA) to the cell surface and promote bacterial uptake into the brain endothelium (1, 6–12). We observed that infection of iPSC-derived BMECs with these previously generated and described GBS mutant strains resulted in significant decreases in the numbers of adherent and/or intracellular bacteria recovered compared to the results for the wild-type parental GBS strains recovered (Fig. 2). Thus, these data demonstrate that these mutant GBS strains exhibited the expected attenuated attachment and invasion phenotypes using iPSC-derived BMECs.

iPSC-derived BMECs are activated in response to GBS infection. Previous reports have shown that the major proinflammatory BBB response to GBS infection is the upregulation of chemokines and cytokines that promote neutrophilic influx (7, 18).

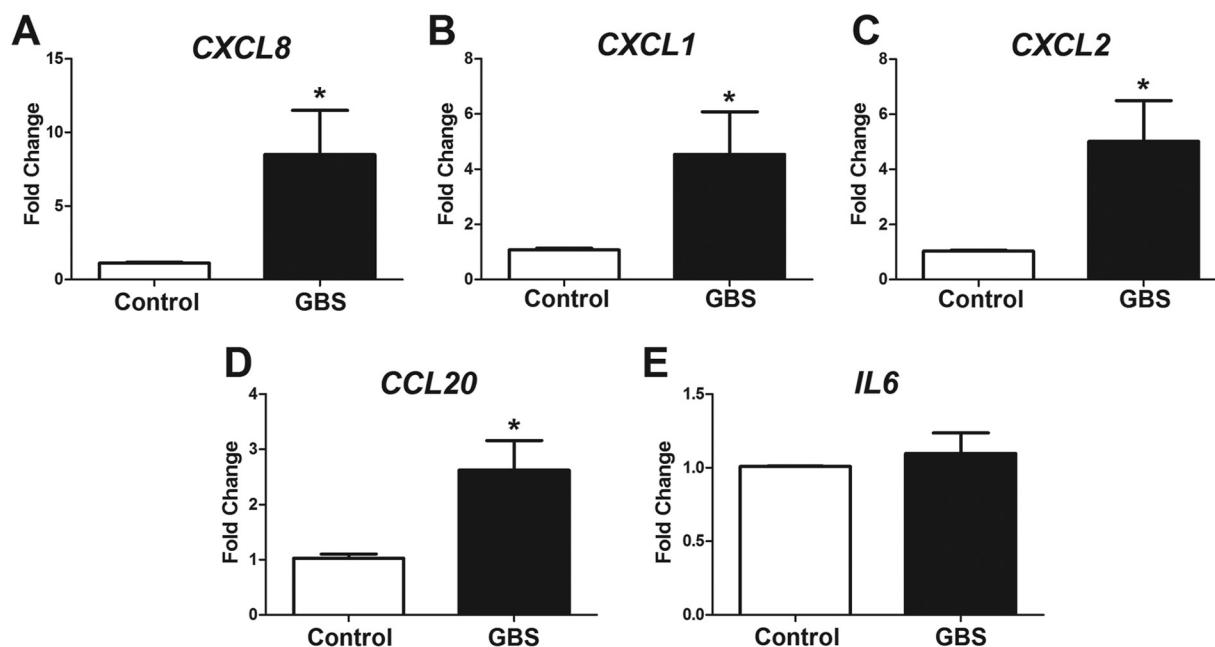


FIG 3 GBS induced activation of iPSC-derived BMECs. Quantitative PCR was performed on iPSC-derived BMECs with or without wild-type GBS infection at an MOI of 10 for 5 h. Neutrophil chemoattractant-coding genes *CXCL8* (IL-8) (A), *CXCL1* (CXCL-1) (B), and *CXCL2* (CXCL-2) (C) and proinflammatory cytokine-coding genes *CCL20* (CCL-20) (D) and *IL6* (IL-6) (E) were evaluated. Data are presented as mean fold changes compared to the results for uninfected controls for at least three independent iPSC-derived BMEC differentiations conducted in triplicate. Error bars represent SEM. Student's *t* test was used to determine significance. *, $P < 0.01$.

Thus, the transcript expression of key chemokines in iPSC-derived BMECs was evaluated following GBS infection. Wild-type GBS at an MOI of 10 was used to infect iPSC-derived BMECs for 5 h, and no loss in cell viability was observed under these conditions (Fig. S3). We observed that *CXCL8* (encoding interleukin-8 [IL-8]), *CXCL1*, and *CXCL2*, as well as *CCL20*, encoding neutrophil chemoattractants, were significantly upregulated in response to GBS infection compared to their levels in the noninfected control (Fig. 3A to D). In contrast, the expression of the gene encoding the global proinflammatory cytokine IL-6 was unchanged in response to GBS infection (Fig. 3E). Together, these data show that key proinflammatory chemokines are induced in iPSC-derived BMECs during GBS infection.

GBS infection disrupts tight junctions of iPSC-derived BMECs. It is known that GBS infection can affect tight junction components and BBB barrier function (17). To determine whether iPSC-derived BMECs were affected by GBS interactions, we used TEER to measure barrier integrity. After 3 h post-GBS infection, we observed a dramatic decrease in the barrier function of iPSC-derived BMECs (Fig. 4A). Tight junction dysfunction during GBS infection was recently reported to be linked to the expression of the tight junction transcriptional repressor Snail1 (*SNAI1*) (17). Consistent with this finding, upregulation of *SNAI1* transcript expression was observed in iPSC-derived BMECs following GBS infection (Fig. 4B). Transcripts for genes encoding tight junction proteins occludin (*OCLN*), claudin-5 (*CLDN5*), and ZO-1 (*TJP1*) were all also decreased during GBS exposure (Fig. 4C to E). The transcript downregulation corresponded to a loss of tight junction complexes, as immunostaining revealed that occludin, claudin-5, and ZO-1 proteins were noticeably discontinuous or absent from cell-cell junctions following infection (Fig. 5A to C). Quantitation using the area fraction index indicated that this decrease was significant compared to the results for the uninfected control (Fig. 5D to F). In contrast, an immortalized hBMEC cell line exhibited a lack of tight junction continuity and did not express claudin-5 (Fig. S4A to E), which is consistent with previous studies using this cell line to examine GBS infection (17). Taken together, these results demonstrate that GBS infection results in the disruption of tight junctions in iPSC-derived BMECs.

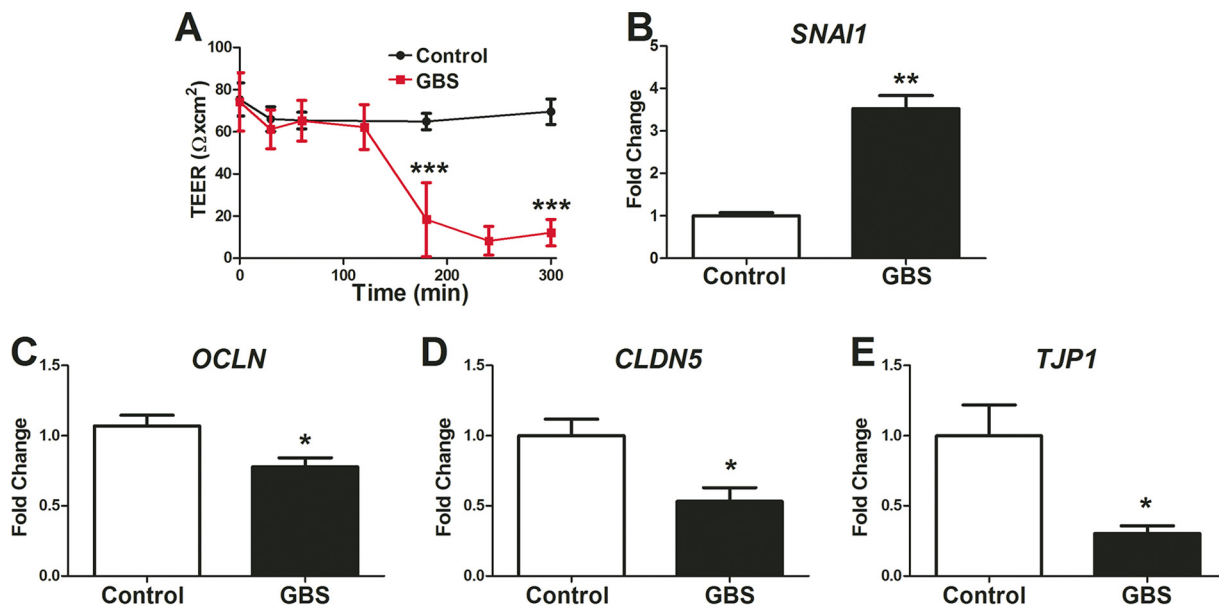


FIG 4 GBS induced BBB disruption on iPSC-derived BMECs. (A) TEER profile during wild-type GBS infection at an MOI of 10. (B to E) Quantitative PCR evaluation of iPSC-derived BMECs infected with wild-type GBS at an MOI of 10 for 5 h. Transcripts of *Snai1* (*SNAI1*) (B), occludin (*OCLN*) (C), claudin-5 (*CLDN5*) (D), and ZO-1 (*TJP1*) (E) were monitored. qPCR data are presented as mean fold changes compared to the results for uninfected controls for at least three independent iPSC-derived BMEC differentiations conducted in triplicate. Error bars represent SEM. Student's *t* test was used to determine significance. *, *P* < 0.05; **, *P* < 0.01; ***, *P* < 0.001.

DISCUSSION

Here, we demonstrate for the first time the use of iPSC-derived BMECs to model the critical steps of bacterial-brain endothelial interactions that lead to BBB penetration and the development of bacterial meningitis. Until now, *in vitro* studies of bacterium-BBB interactions have largely relied on immortalized human BMECs (hBMECs) (6–8, 12, 15, 17, 18, 24, 30, 31, 45, 47–52). While the immortalized hBMECs offered the ability to begin understanding the molecular interactions leading to BBB penetration, the model itself lacks important BBB properties, such as the proper expression and localization of tight junction proteins (Fig. S4) (17). More recently, other immortalized human BBB models, such as the human cerebral microvascular endothelial cell (hCMEC) line hCMEC/D3, have been developed. In contrast to the immortalized hBMECs described here, hCMEC/D3s do express junctional claudin-5; however, occludin expression is discontinuous, leading to modest TEERs (~40 Ω × cm²) that are not substantially improved upon coculture with astrocytes (35, 36, 53–56). Similar to immortalized human BMEC lines, the iPSC-derived BMEC model offers a reliable and scalable method of generating BMECs that express BBB markers. iPSC-derived BMECs offer the additional advantages of continuous tight junctions, barrier formation, and elevated TEER in response to astrocyte cues (Fig. S1) (29, 38, 40, 57). Furthermore, the addition of retinoic acid to the iPSC-derived BMEC differentiation can greatly elevate TEER values, to physiological levels (38, 40). Our results suggest that the iPSC-derived BMEC model can be utilized to study bacterial attachment, invasion, immune activation, and tight junction disruption using GBS as a model meningeal pathogen. In addition, our data compare well with published data regarding attachment and invasion percentages using the immortalized BMEC models. Previous work has demonstrated a range of GBS attachment of between 15 and 28%, with intracellular CFU in the range of 2.5 to 4% (11, 12, 47); in the present study, we observed comparable percentages. This new model may also be helpful for future studies examining other bacterial meningeal pathogens, such as *Streptococcus pneumoniae* (pneumococcus), *Neisseria meningitidis* (meningococcus), and *Escherichia coli* strain K1.

The physical interaction between GBS and brain endothelial cells has been characterized previously using immortalized human BMECs (1). GBS possesses the ability to

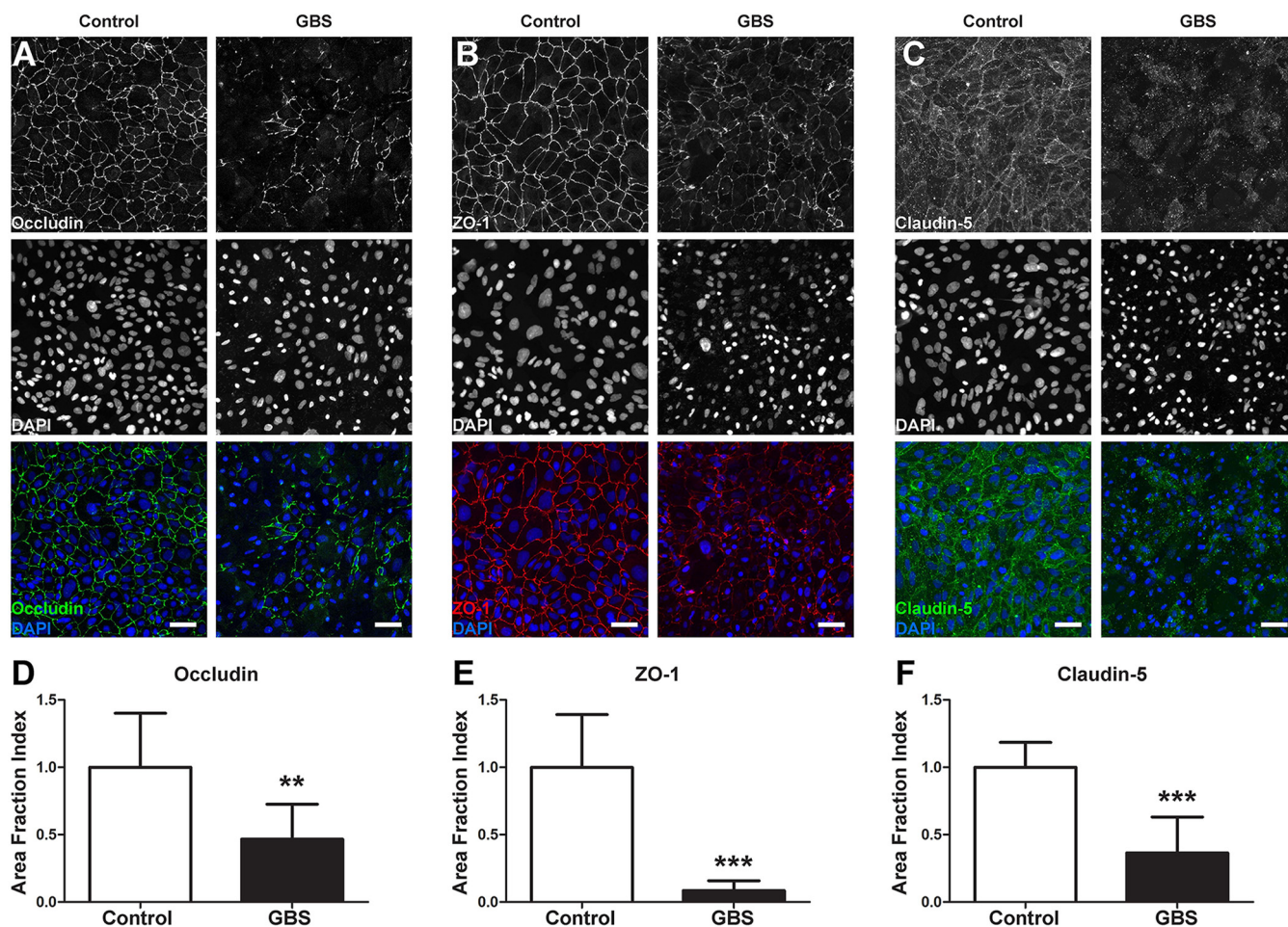


FIG 5 GBS induced tight junction disruption in iPSC-derived BMECs. iPSC-derived BMECs were stained for tight junction proteins following GBS infection, and the results were compared to those for the uninfected control. (A to C) Representative images of occludin (A), ZO-1 (B), and claudin-5 (C) staining. Scale bars represent 50 μm . (D to F) Area fraction indices of occludin (D), ZO-1 (E), and claudin-5 (F) staining after GBS infection. Area fraction index data are presented as the mean values of at least six independent images taken from at least two independent differentiations, with three images taken per differentiation. Error bars represent SD. Student's *t* test was used to determine significance. *, $P < 0.05$; **, $P < 0.01$; ***, $P < 0.001$.

adhere to and invade brain endothelial cells through the use of a variety of virulence factors, such as the PilA, SfbA, Srr2, and lagA proteins (6–12). Our results demonstrate that these factors also contribute to bacterial interaction with the iPSC-derived BMECs. Many of the GBS virulence factors we examined are proteins that promote bacterial interaction with ECM components, including collagen (for PilA), fibronectin (for SfbA), and fibrinogen (for Srr2). These interactions are thought to allow GBS to bridge to host cell receptors directly, promoting bacterial attachment and invasion of multiple host cell types, including brain endothelial cells (7, 9, 12). Here, we show that these adhesins also promote GBS interaction with iPSC-derived BMECs, suggesting that the iPSC-derived BMECs maintain similar cellular receptors necessary for GBS attachment. As it has been previously thought that attachment would precede invasion, it is then unsurprising that adhesion deficiencies, such as in the case of PilA, may also result in a decrease in invasion. Studies have also described a role for lagA, a glycosyltransferase that acts to generate the glycolipid anchor for LTA, in the pathogenesis of GBS using immortalized BMECs *in vitro* and a mouse model of GBS infection. Our results support these previous findings, as the ΔlagA mutant was less invasive with the iPSC-derived BMECs, although we observed that the ΔlagA mutant also had reduced adherent properties. It is unknown at this point whether the deletion of *lagA* only impacts anchored LTA or whether other surface factors are disrupted in the ΔlagA mutant that may impact GBS-BBB interactions. The work characterizing GBS SfbA in immortalized

hBMECs has demonstrated its contribution to bacterial entry (12), while we observed a role for both attachment and invasion of iPSC-derived BMECs. Interestingly, SfbA is a homolog of the pneumococcal adhesin PavaA, previously shown to contribute to pneumococcal adherence to BMECs (58, 59), and therefore, it is possible that SfbA could be contributing to GBS adherence, which is better detected in the iPSC-derived model. Additionally SfbA has been reported to contribute to GBS adherence to fibronectin (12), and the binding of extracellular matrix as a means to adhere to host BBB has been discussed previously (7, 13, 49). Regardless, our results demonstrate that known GBS mutants are attenuated in their interaction with iPSC-derived BMECs, suggesting that in general, similar mechanisms for bacterial-host cell interactions are preserved in the iPSC-derived-BMEC model.

Bacterial activation of the brain endothelium has been hypothesized to contribute to disease progression through the upregulation of cytokines and chemokines that attract circulating leukocytes, specifically neutrophils (1–5). Previous work has demonstrated that the recruitment of neutrophils contributes to further BBB destruction in murine models of GBS meningitis (7). As expected, in response to GBS infection, iPSC-derived BMECs upregulate *CXCL8* (IL-8), *CXCL1*, and *CXCL2*, encoding potent neutrophil chemoattractants. Our findings agree with published results on the immortalized BMEC models, where the expression levels of *CXCL8*, *CXCL1*, and *CXCL2* were upregulated between 6- and 15-fold (7). Interestingly, however, we did not observe upregulation of *IL6*, encoding the global proinflammatory cytokine IL-6. It is possible that IL-6 may be generated from other sources besides the brain endothelium *in vivo*, given that it is detected at high levels in the sera of infected animals (7). Further investigation is needed to determine the overall transcriptional profile of iPSC-derived BMECs during GBS infection. However, GBS infection of iPSC-derived BMECs induced a set of chemokines that act to orchestrate neutrophil recruitment and activation.

We recently demonstrated that GBS is able to induce the expression of the transcriptional repressor of tight junctions, Snail1, which contributes to tight junction disruption in immortalized hBMECs during GBS infection (17). In agreement with these findings, GBS infection of iPSC-derived BMECs upregulated Snail1 and substantially decreased the tight junctional continuity and resultant barrier properties. Furthermore, our previous work examining tight junction disruption was limited by the use of immortalized human BMEC cell lines that did not express claudin-5 and lacked continuous occludin staining and, thus, lacked an optimal barrier phenotype (Fig. S4) (17). The iPSC-derived BMECs express claudin-5 and have properly localized occludin and, thus, allow for the much more relevant analysis of tight junction function during GBS infection.

In vivo, BMECs are supported by a number of other CNS cell types, such as the astrocytes, neurons, and pericytes that make up the NVU. Currently, little is known about the contribution of astrocytes, neurons, and pericytes to BBB function during meningitis. Models combining iPSC-derived neurons and astrocytes along with iPSC-derived BMECs have been reported by us and others (29, 34, 35, 37, 38, 57, 60). Combined with this report establishing iPSC-derived BMECs as a model to study bacterial meningitis, these tools will likely support future studies examining the role of other NVU cell types and their contributions during infection.

MATERIALS AND METHODS

Bacterial strains and cell lines used. Group B *Streptococcus* (GBS; *Streptococcus agalactiae*) hyper-virulent clinical isolates COH1 (serotype III, multilocus sequence type 17 [MLST-17]) (61) and NCTC10/84 (serotype V, MLST-26) (62) were used. COH1 $\Delta iagA$ (6), $\Delta srr2$ (63, 64), and $\Delta sfbA$ (12) and NCTC10/84 $\Delta pilA$ (8) mutants have been described previously. GBS strains were all grown in Todd-Hewitt broth (THB) at 37°C. *Lactococcus lactis* was grown in M17 medium at 30°C (8). iPSC line DF19-9-11 (WiCell) was chosen for this study as this iPSC line was not generated through the use of viral integration vectors, eliminating the potential for inherent antiviral or anti-inflammatory responses. DF19-9-11 cells were grown in mTeSR1 medium (WiCell) that was changed daily and maintained on Matrigel (WiCell)-coated plates (Corning) consistent with previously published methods (29, 38–40, 57). Immortalized hBMECs (a gift of Kwang Sik Kim and Monique Stins, Johns Hopkins University, Baltimore, MD) were cultured in RPMI 1640

containing 10% fetal bovine serum (FBS), 10% NuSerum, and 1% nonessential amino acids as described previously (6, 7, 12, 17, 31).

Generation of BMECs and astrocytes from iPSCs. DF19-9-11 iPSCs were differentiated into BMECs according to methods published previously (29, 38–40, 57). Briefly, a single-cell suspension of iPSCs was seeded at a density of 10,000/cm² onto Matrigel (WiCell) cell culture plates or flasks (Corning) and grown for 3 days. Differentiation was initiated by changing to UM medium (Dulbecco modified Eagle medium [DMEM]–F-12 medium plus 20% knockout serum replacement [KOSR], 1% minimal essential medium [MEM], 0.5% Glutamax, and 0.07% beta-mercaptoethanol) for 6 days, refreshing the medium daily. The medium was then changed to EC medium (human endothelial cell serum-free medium plus 1% platelet-poor plasma-derived serum [Fisher] and 500 ng/ml basic fibroblast growth factor [bFGF]) for 2 days. Finally, BMECs were purified on fibronectin- and collagen-coated plates or Transwell inserts (Corning, product number 3460). BMECs were analyzed for TEER using an EVOM II instrument (World Precision) and for the expression of endothelial markers as described previously (29, 40). The addition of retinoic acid during BMEC differentiation has been shown to elevate BBB properties, including TEER and vascular endothelial (VE)-cadherin expression (38, 39). However, since retinoic acid has been shown to have anti-inflammatory properties and could interfere with cellular responses to bacteria (65–69), it was not used. Astrocytes were generated as described previously (57).

Infection assays. iPSC-derived BMECs purified onto collagen-fibronectin-coated 24-well plates (Corning) were grown to a confluent monolayer. A multiplicity of infection (MOI) of 10 was used for all experiments unless noted specifically. Overnight cultures of GBS or *L. lactis* were grown in THB or M17, respectively, subcultured the following day, and grown to an optical density at 600 nm (OD₆₀₀) of 0.4. Bacteria were spun down and washed in phosphate-buffered saline (PBS) prior to infecting BMECs. Enumeration of total cell-associated and intracellular CFU was performed as described previously (6, 7, 31). Briefly, for adherence, bacteria were incubated with BMECs for 30 min at 37°C and 5% CO₂, followed by 5 washes in PBS. Mammalian cells were lysed in 0.025% Triton X-100 and plated in a dilution series onto THB plates (M17 for *L. lactis*) to determine bacterial loads. For invasion, bacteria were incubated at 37°C and 5% CO₂ for 2 h, followed by 3 washes in PBS and incubation with antibiotic medium for an additional 2 h at 37°C and 5% CO₂. After the second 2-h incubation, BMECs were lysed in 0.025% Triton X-100 and plated in a dilution series onto THB plates (M17 for *L. lactis*) to determine bacterial loads. Intracellular survival assays were run exactly like the intracellular assessment assays; however, cultures were incubated in antibiotic medium for extended periods of time as described previously (45). The following day, bacterial loads were determined by counting the colonies of countable dilutions and back calculating. Data are presented as total CFU recovered or as the percentage of the initial inoculum.

RNA isolation and quantitative PCR. iPSC-derived BMECs were infected with GBS for 5 h at 37°C and 5% CO₂. Following infection, cell lysates were collected for RNA isolation in lysis buffer (PureLink RNA minikit; Life Technologies, Inc.). RNA was purified using the PureLink RNA minikit (Life Technologies, Inc.), and cDNA was generated utilizing the Vilo first-strand kit (Life Technologies, Inc.). SYBR green (Thermo Fisher) quantitative PCR (qPCR) for *CXCL8* (IL-8), *CXCL1*, *CXCL2*, *CCL20*, *IL6*, *GAPDH* (glyceraldehyde-3-phosphate dehydrogenase [GAPDH]), and *SNAIL1* (Snail1) was conducted using previously described primers (6, 17, 24). TaqMan probes (Thermo Fisher) were used for detection of *TJP1* (ZO-1) (Hs0155186_m1), *CLDN5* (claudin-5) (Hs00533949_s1), *OCLN* (occludin) (Hs00170162_m1), and *GAPDH* (Hs02786624_g1). qPCR data were collected on a BioRad CFX96 thermocycler, and data are presented as fold change over the results for *GAPDH* using the cycle threshold ($\Delta\Delta C_T$) calculation.

Immunofluorescence and area fraction index calculations. Immortalized hBMECs and iPSC-derived BMECs were either infected with GBS for 5 h at 37°C and 5% CO₂ or left uninfected as controls. After infection, cells were fixed and stained exactly as reported previously (40), with the single exception that anti-ZO-1 antibody (catalog number 339100; Thermo Scientific) was used in place of the previously reported anti-ZO-1 antibody. Briefly, BMECs were fixed in 100% ice-cold methanol and stained overnight at 4°C. Secondary antibodies were utilized at a 1:200 dilution, and samples were visualized with an Olympus IX70 inverted fluorescence microscope using Nikon NIS image acquisition software. Fiji ImageJ was used to create merged images. Determination of the area fraction index of tight junction staining and continuity was performed as described previously (57). Using Fiji ImageJ, images were corrected for inconsistent fluorescence illumination using the Background Correction plugin. Next, the gray scale intensity profile was examined to determine a threshold value that minimizes background while maintaining the staining profile. Images were then converted to a binary image and processed using the outline filter to determine the perimeter of tight junction staining in pixels. Total pixels were normalized to the square root of the number of cells in the image.

Flow cytometry. To assay the expression of the $\beta 1$ integrin, iPSC-derived BMECs were differentiated, fixed in 1% paraformaldehyde, and stained using a 1:1,000 dilution of anti- $\beta 1$ integrin antibody (catalog number NB100-63255; Abcam, Inc.) in 0.5% bovine serum albumin (BSA) in PBS overnight at 4°C. The following day, fixed cells were washed in 0.5% BSA in PBS twice and stained with anti-mouse IgG Alexa Fluor 488 antibody (catalog number A-11001; Life Technologies, Inc.) for 1 h at room temperature. Cells were then washed twice in 0.5% BSA in PBS and run on a BD Accuri C6 flow cytometry instrument for fluorescence-activated cell sorting (FACS) analysis.

Western blot analysis. Immortalized hBMECs and iPSC-derived BMECs were infected as described above for 5 h at an MOI of 10. Then, cells were washed three times in sterile PBS, and cell lysates were taken using radioimmunoprecipitation assay (RIPA) buffer plus protease inhibitor cocktail (catalog number 78443; Thermo Scientific). Proteins were quantified using a bicinchoninic acid (BCA) assay (catalog number 23227; Thermo Scientific), and equal amounts were loaded onto protein gels and

transferred to nitrocellulose membranes. Anti-COX IV antibody was used as a protein loading control (catalog number 4850T; Cell Signaling Technologies), and anti-claudin-5 antibody (catalog number 35-2500; Thermo Scientific) to visualize claudin-5. Horseradish peroxidase (HRP)-conjugated secondary antibodies (Jackson Laboratory) and a BioRad ChemiDoc XRS+ instrument were used to image the blots.

Statistics. GraphPad Prism version 5.0 (GraphPad Software, Inc.) was used for all statistical analysis. For pairwise comparisons, the 2-tailed Student *t* test was used where appropriate. For multiple comparisons, analysis of variance (ANOVA) was used to determine statistics. Data are represented as mean values \pm standard errors of the means (SEM) where triplicate mean values are presented and as mean values \pm standard deviations (SD) where raw values are presented. Statistical significance was accepted at a *P* value of less than 0.05.

SUPPLEMENTAL MATERIAL

Supplemental material for this article may be found at <https://doi.org/10.1128/mSphere.00398-17>.

FIG S1, PDF file, 0.5 MB.

FIG S2, PDF file, 0.02 MB.

FIG S3, PDF file, 0.01 MB.

FIG S4, PDF file, 2.6 MB.

ACKNOWLEDGMENTS

This work was supported by Defense Threat Reduction Agency grant HDTRA1-15-0047 and National Institutes of Health grants R01NS083688 to E.V.S. and R01-NS051247 to K.S.D. B.J.K. was partially supported by a postdoctoral training fellowship from the Stem Cell Regenerative Medicine Center at the University of Wisconsin. M.A.M. was partially supported by a Wisconsin Stem Cell Roundtable fellowship at the University of Wisconsin.

B.J.K., O.B.B., and M.A.M. conducted experiments and collected data. B.J.K. and M.J.S. collected and analyzed area fraction index results. B.J.K., K.S.D., S.P.P., and E.V.S. provided materials, input on data analysis, and input on data interpretation. B.J.K., K.S.D., and E.V.S. contributed to experimental design and wrote the paper.

REFERENCES

- Doran KS, Fulde M, Gratz N, Kim BJ, Nau R, Prasadarao N, Schubert-Unkmeir A, Tuomanen El, Valentin-Weigand P. 2016. Host–pathogen interactions in bacterial meningitis. *Acta Neuropathol* 131:185–209. <https://doi.org/10.1007/s00401-015-1531-z>.
- Kim KS. 2006. Microbial translocation of the blood-brain barrier. *Int J Parasitol* 36:607–614. <https://doi.org/10.1016/j.ijpara.2006.01.013>.
- van Sorge NM, Doran KS. 2012. Defense at the border: the blood-brain barrier versus bacterial foreigners. *Future Microbiol* 7:383–394. <https://doi.org/10.2217/fmb.12.1>.
- Maisey HC, Doran KS, Nizet V. 2008. Recent advances in understanding the molecular basis of group B *Streptococcus* virulence. *Expert Rev Mol Med* 10:e27. <https://doi.org/10.1017/S1462399408000811>.
- Doran KS, Nizet V. 2004. Molecular pathogenesis of neonatal group B streptococcal infection: no longer in its infancy. *Mol Microbiol* 54:23–31. <https://doi.org/10.1111/j.1365-2958.2004.04266.x>.
- Doran KS, Engelson EJ, Khosravi A, Maisey HC, Fedtke I, Equils O, Michelsen KS, Arditi M, Peschel A, Nizet V. 2005. Blood-brain barrier invasion by group B *Streptococcus* depends upon proper cell-surface anchoring of lipoteichoic acid. *J Clin Invest* 115:2499–2507. <https://doi.org/10.1172/JCI23829>.
- Banerjee A, Kim BJ, Carmona EM, Cutting AS, Gurney MA, Carlos C, Feuer R, Prasadarao NV, Doran KS. 2011. Bacterial pili exploit integrin machinery to promote immune activation and efficient blood-brain barrier penetration. *Nat Commun* 2:462. <https://doi.org/10.1038/ncomms1474>.
- Maisey HC, Hensler M, Nizet V, Doran KS. 2007. Group B streptococcal pilus proteins contribute to adherence to and invasion of brain microvascular endothelial cells. *J Bacteriol* 189:1464–1467. <https://doi.org/10.1128/JB.01153-06>.
- Seo HS, Minasov G, Seepersaud R, Doran KS, Dubrovskaya I, Shuvalova L, Anderson WF, Iverson TM, Sullam PM. 2013. Characterization of fibrinogen binding by glycoproteins Srr1 and Srr2 of *Streptococcus agalactiae*. *J Biol Chem* 288:35982–35996. <https://doi.org/10.1074/jbc.M113.513358>.
- Six A, Bellais S, Bouaboud A, Fouet A, Gabriel C, Tazi A, Dramsi S, Trieu-Cuot P, Poyart C. 2015. Srr2, a multifaceted adhesin expressed by ST-17 hypervirulent group B *Streptococcus* involved in binding to both fibrinogen and plasminogen. *Mol Microbiol* 97:1209–1222. <https://doi.org/10.1111/mmi.13097>.
- van Sorge NM, Quach D, Gurney MA, Sullam PM, Nizet V, Doran KS. 2009. The group B streptococcal serine-rich repeat 1 glycoprotein mediates penetration of the blood-brain barrier. *J Infect Dis* 199:1479–1487. <https://doi.org/10.1086/598217>.
- Mu R, Kim BJ, Paco C, Del Rosario YD, Courtney HS, Doran KS. 2014. Identification of a group B streptococcal fibronectin binding protein, SfbA, that contributes to invasion of brain endothelium and development of meningitis. *Infect Immun* 82:2276–2286. <https://doi.org/10.1128/IAI.01559-13>.
- Tenenbaum T, Bloier C, Adam R, Reinscheid DJ, Schrotten H. 2005. Adherence to and invasion of human brain microvascular endothelial cells are promoted by fibrinogen-binding protein FbsA of *Streptococcus agalactiae*. *Infect Immun* 73:4404–4409. <https://doi.org/10.1128/IAI.73.7.4404-4409.2005>.
- Tazi A, Disson O, Bellais S, Bouaboud A, Dmytruk N, Dramsi S, Mistou MY, Khun H, Mechler C, Tardieux I, Trieu-Cuot P, Lecuit M, Poyart C. 2010. The surface protein HvgA mediates group B streptococcus hypervirulence and meningeal tropism in neonates. *J Exp Med* 207:2313–2322. <https://doi.org/10.1084/jem.20092594>.
- Lembo A, Gurney MA, Burnside K, Banerjee A, De Los Reyes M, Connelly JE, Lin WJ, Jewell KA, Vo A, Renken CW, Doran KS, Rajagopal L. 2010. Regulation of CovR expression in group B *Streptococcus* impacts blood-brain barrier penetration. *Mol Microbiol* 77:431–443. <https://doi.org/10.1111/j.1365-2958.2010.07215.x>.
- Quach D, Van Sorge NM, Kristian SA, Bryan JD, Shelver DW, Doran KS. 2009. The CiaR response regulator in group b streptococcus promotes intracellular survival and resistance to innate immune defenses. *J Bacteriol* 191:2023–2032. <https://doi.org/10.1128/JB.01216-08>.
- Kim BJ, Hancock BM, Bermudez A, Del Cid N, Reyes E, Van Sorge NM, Lauth X, Smurthwaite CA, Hilton BJ, Stotland A, Banerjee A, Buchanan J, Wolkowicz R, Traver D, Doran KS. 2015. Bacterial induction of Snail1

- contributes to blood-brain barrier disruption. *J Clin Invest* 125: 2473–2483. <https://doi.org/10.1172/JCI74159>.
18. Doran KS, Liu GY, Nizet V. 2003. Group B streptococcal β -hemolysin/cytolysin activates neutrophil signaling pathways in brain endothelium and contributes to development of meningitis. *J Clin Invest* 112: 736–744. <https://doi.org/10.1172/JCI17335>.
 19. Abbott NJ. 2013. Blood-brain barrier structure and function and the challenges for CNS drug delivery. *J Inher Metab Dis* 36:437–449. <https://doi.org/10.1007/s10545-013-9608-0>.
 20. Abbott NJ, Patabendige AAK, Dolman DEM, Yusof SR, Begley DJ. 2010. Structure and function of the blood-brain barrier. *Neurobiol Dis* 37: 13–25. <https://doi.org/10.1016/j.nbd.2009.07.030>.
 21. Abbott NJ, Rönnbäck L, Hansson E. 2006. Astrocyte-endothelial interactions at the blood-brain barrier. *Nat Rev Neurosci* 7:41–53. <https://doi.org/10.1038/nrn1824>.
 22. Orihuela CJ, Mahdavi J, Thornton J, Mann B, Wooldridge KG, Abouseada N, Oldfield NJ, Self T, Ala'Aldeen DAA, Tuomanen EI. 2009. Laminin receptor initiates bacterial contact with the blood brain barrier in experimental meningitis models. *J Clin Invest* 119:1638–1646. <https://doi.org/10.1172/JCI36759>.
 23. Garcia-Monco JC, Miller NS, Backenson PB, Anda P, Benach JL. 1997. A mouse model of Borrelia meningitis after intradermal injection. *J Infect Dis* 175:1243–1245. <https://doi.org/10.1086/593681>.
 24. van Sorge NM, Ebrahimi CM, McGillivray SM, Quach D, Sabet M, Guiney DG, Doran KS. 2008. Anthrax toxins inhibit neutrophil signaling pathways in brain endothelium and contribute to the pathogenesis of meningitis. *PLoS One* 3:e2964. <https://doi.org/10.1371/journal.pone.0002964>.
 25. Leib SL, Kim YS, Chow LL, Sheldon RA, Täuber MG. 1996. Reactive oxygen intermediates contribute to necrotic and apoptotic neuronal injury in an infant rat model of bacterial meningitis due to group B streptococci. *J Clin Invest* 98:2632–2639. <https://doi.org/10.1172/JCI119084>.
 26. Liechti FD, Grandgirard D, Leppert D, Leib SL. 2014. Matrix metalloproteinase inhibition lowers mortality and brain injury in experimental pneumococcal meningitis. *Infect Immun* 82:1710–1718. <https://doi.org/10.1128/IAI.00073-14>.
 27. Kim BJ, Hancock BM, Del Cid N, Bermudez A, Traver D, Doran KS. 2015. Streptococcus agalactiae infection in zebrafish larvae. *Microb Pathog* 79:57–60. <https://doi.org/10.1016/j.micpath.2015.01.007>.
 28. Patterson H, Saralahti A, Parikka M, Dramsi S, Trieu-Cuot P, Poyart C, Rounioja S, Rämetsä M. 2012. Adult zebrafish model of bacterial meningitis in Streptococcus agalactiae infection. *Dev Comp Immunol* 38:447–455. <https://doi.org/10.1016/j.dci.2012.07.007>.
 29. Lippmann ES, Azarin SM, Kay JE, Nessler RA, Wilson HK, Al-Ahmad A, Palecek SP, Shusta EV. 2012. Derivation of blood-brain barrier endothelial cells from human pluripotent stem cells. *Nat Biotechnol* 30:783–791. <https://doi.org/10.1038/nbt.2247>.
 30. Schubert-Unkmeir A, Konrad C, Slanina H, Czapek F, Hebling S, Frosch M. 2010. Neisseria meningitidis induces brain microvascular endothelial cell detachment from the matrix and cleavage of occludin: a role for MMP-8. *PLoS Pathog* 6:e1000874. <https://doi.org/10.1371/journal.ppat.1000874>.
 31. Nizet V, Kim KS, Stins M, Jonas M, Chi EY, Nguyen D, Rubens CE. 1997. Invasion of brain microvascular endothelial cells by group B streptococci. *Infect Immun* 65:5074–5081.
 32. Zhe M, Jie P, Hui Z, Bin X, Xiaomeng P, Huixing L, Chengping L, Hongjie F. 2016. SILAC and LC-MS/MS identification of Streptococcus equi ssp. zooepidemicus proteins that contribute to mouse brain microvascular endothelial cell infection. *Appl Microbiol Biotechnol* 100:7125–7136. <https://doi.org/10.1007/s00253-016-7579-4>.
 33. Xiao G, Tang H, Zhang S, Ren H, Dai J, Lai L, Lu C, Yao H, Fan H, Wu Z. 2017. Streptococcus suis small RNA rss04 contributes to the induction of meningitis by regulating capsule synthesis and by inducing biofilm formation in a mouse infection model. *Vet Microbiol* 199:111–119. <https://doi.org/10.1016/j.vetmic.2016.12.034>.
 34. Lippmann ES, Al-Ahmad A, Palecek SP, Shusta EV. 2013. Modeling the blood-brain barrier using stem cell sources. *Fluids Barriers CNS* 10:2. <https://doi.org/10.1186/2045-8118-10-2>.
 35. Helms HC, Abbott NJ, Burek M, Cecchelli R, Couraud PO, Deli MA, Förster C, Galla HJ, Romero IA, Shusta EV, Stebbins MJ, Vandenhaute E, Weksler B, Brodin B. 2016. *In vitro* models of the blood-brain barrier: an overview of commonly used brain endothelial cell culture models and guidelines for their use. *J Cereb Blood Flow Metab* 36:862–890. <https://doi.org/10.1177/0271678X16630991>.
 36. Rahman NA, Rasil ANHM, Meyding-Lamade U, Craemer EM, Diah S, Tuah AA, Muharram SH. 2016. Immortalized endothelial cell lines for in vitro blood-brain barrier models: a systematic review. *Brain Res* 1642:532–545. <https://doi.org/10.1016/j.brainres.2016.04.024>.
 37. Hollmann EK, Bailey AK, Potharazu AV, Neely MD, Bowman AB, Lippmann ES. 2017. Accelerated differentiation of human induced pluripotent stem cells to blood-brain barrier endothelial cells. *Fluids Barriers CNS* 14:9. <https://doi.org/10.1186/s12987-017-0059-0>.
 38. Lippmann ES, Al-Ahmad A, Azarin SM, Palecek SP, Shusta EV. 2014. A retinoic acid-enhanced, multicellular human blood-brain barrier model derived from stem cell sources. *Sci Rep* 4:4160. <https://doi.org/10.1038/srep04160>.
 39. Wilson HK, Canfield SG, Hjortness MK, Palecek SP, Shusta EV. 2015. Exploring the effects of cell seeding density on the differentiation of human pluripotent stem cells to brain microvascular endothelial cells. *Fluids Barriers CNS* 12:13. <https://doi.org/10.1186/s12987-015-0007-9>.
 40. Stebbins MJ, Wilson HK, Canfield SG, Qian T, Palecek SP, Shusta EV. 2016. Differentiation and characterization of human pluripotent stem cell-derived brain microvascular endothelial cells. *Methods* 101:93–102. <https://doi.org/10.1016/j.jymeth.2015.10.016>.
 41. Vatine GD, Al-Ahmad A, Barriga BK, Svendsen S, Salim A, Garcia L, Garcia VJ, Ho R, Yucer N, Qian T, Lim RG, Wu J, Thompson LM, Spivia WR, Chen Z, Van Eyk J, Palecek SP, Refetoff S, Shusta EV, Svendsen CN. 2017. Modeling psychomotor retardation using iPSCs from MCT8-deficient patients indicates a prominent role for the blood-brain barrier. *Cell Stem Cell* 20:831–843.e5. <https://doi.org/10.1016/j.stem.2017.04.002>.
 42. Lim RG, Quan C, Reyes-Ortiz AM, Lutz SE, Kedaigle AJ, Gipson TA, Wu J, Vatine GD, Stocksdale J, Casale MS, Svendsen CN, Fraenkel E, Housman DE, Agalliu D, Thompson LM. 2017. Huntington's disease iPSC-derived brain microvascular endothelial cells reveal WNT-mediated angiogenic and blood-brain barrier deficits. *Cell Rep* 19:1365–1377. <https://doi.org/10.1016/j.celrep.2017.04.021>.
 43. Clark PA, Al-Ahmad AJ, Qian T, Zhang RR, Wilson HK, Weichert JP, Palecek SP, Kuo JS, Shusta EV. 2016. Analysis of cancer-targeting alkylphosphocholine analog permeability characteristics using a human induced pluripotent stem cell blood-brain barrier model. *Mol Pharm* 13:3341–3349. <https://doi.org/10.1021/acs.molpharmaceut.6b00441>.
 44. Kokubu Y, Yamaguchi T, Kawabata K. 2017. In vitro model of cerebral ischemia by using brain microvascular endothelial cells derived from human induced pluripotent stem cells. *Biochem Biophys Res Commun* 486:577–583. <https://doi.org/10.1016/j.bbrc.2017.03.092>.
 45. Cutting AS, Del Rosario Y, Mu R, Rodriguez A, Till A, Subramani S, Gottlieb RA, Doran KS. 2014. The role of autophagy during group B Streptococcus infection of blood-brain barrier endothelium. *J Biol Chem* 289:35711–35723. <https://doi.org/10.1074/jbc.M114.588657>.
 46. Cumley NJ, Smith LM, Anthony M, May RC. 2012. The CovS/CovR acid response regulator is required for intracellular survival of group B Streptococcus in macrophages. *Infect Immun* 80:1650–1661. <https://doi.org/10.1128/IAI.05443-11>.
 47. Mu R, Cutting AS, Del Rosario Y, Villarino N, Stewart L, Weston TA, Patras KA, Doran KS. 2016. Identification of CiaR regulated genes that promote group B streptococcal virulence and interaction with brain endothelial cells. *PLoS One* 11:e0153891. <https://doi.org/10.1371/journal.pone.0153891>.
 48. Maruvada R, Kim KS. 2012. IbeA and OmpA of Escherichia coli K1 exploit Rac1 activation for invasion of human brain microvascular endothelial cells. *Infect Immun* 80:2035–2041. <https://doi.org/10.1128/IAI.06320-11>.
 49. Slanina H, Hebling S, Hauck CR, Schubert-Unkmeir A. 2012. Cell invasion by Neisseria meningitidis requires a functional interplay between the focal adhesion kinase, Src and cortactin. *PLoS One* 7:e39613. <https://doi.org/10.1371/journal.pone.0039613>.
 50. Banerjee A, van Sorge NM, Sheen TR, Uchiyama S, Mitchell TJ, Doran KS. 2010. Activation of brain endothelium by pneumococcal neuraminidase NanA promotes bacterial internalization. *Cell Microbiol* 12:1576–1588. <https://doi.org/10.1111/j.1462-5822.2010.01490.x>.
 51. Huang SH, Wass C, Fu Q, Prasadarao NV, Stins M, Kim KS. 1995. Escherichia coli invasion of brain microvascular endothelial cells in vitro and in vivo: molecular cloning and characterization of invasion gene ibe10. *Infect Immun* 63:4470–4475.
 52. Uchiyama S, Carlin AF, Khosravi A, Weiman S, Banerjee A, Quach D, Hightower G, Mitchell TJ, Doran KS, Nizet V. 2009. The surface-anchored NanA protein promotes pneumococcal brain endothelial cell invasion. *J Exp Med* 206:1845–1852. <https://doi.org/10.1084/jem.20090386>.
 53. Förster C, Burek M, Romero IA, Weksler B, Couraud PO, Drenckhahn D. 2008. Differential effects of hydrocortisone and TNF α on tight junctions.

- tion proteins in an in vitro model of the human blood-brain barrier. *J Physiol* 586:1937–1949. <https://doi.org/10.1113/jphysiol.2007.146852>.
54. Wilson HK, Shusta EV. 2015. Human-based in vitro brain endothelial cell models, p 238–273. *In* Di L, Kerns EH (ed), *Blood-brain barrier in drug discovery: optimizing brain exposure of CNS drugs and minimizing brain side effects for peripheral drugs*. John Wiley and Sons, Hoboken, NJ.
 55. Hatherell K, Couraud PO, Romero IA, Weksler B, Pilkington GJ. 2011. Development of a three-dimensional, all-human in vitro model of the blood-brain barrier using mono-, co-, and tri-cultivation Transwell models. *J Neurosci Methods* 199:223–229. <https://doi.org/10.1016/j.jneumeth.2011.05.012>.
 56. Weksler BB, Subileau EA, Perrière N, Charneau P, Holloway K, Leveque M, Tricoire-Leignel H, Nicotra A, Bourdoulous S, Turowski P, Male DK, Roux F, Greenwood J, Romero IA, Couraud PO. 2005. Blood-brain barrier-specific properties of a human adult brain endothelial cell line. *FASEB J* 19:1872–1874. <https://doi.org/10.1096/fj.04-3458fje>.
 57. Canfield SG, Stebbins MJ, Morales BS, Asai SW, Vatine GD, Svendsen CN, Palecek SP, Shusta EV. 2017. An isogenic blood-brain barrier model comprising brain endothelial cells, astrocytes, and neurons derived from human induced pluripotent stem cells. *J Neurochem* 140:874–888. <https://doi.org/10.1111/jnc.13923>.
 58. Holmes AR, McNab R, Millsap KW, Rohde M, Hammerschmidt S, Mawdsley JL, Jenkinson HF. 2001. The pavA gene of *Streptococcus pneumoniae* encodes a fibronectin-binding protein that is essential for virulence. *Mol Microbiol* 41:1395–1408. <https://doi.org/10.1046/j.1365-2958.2001.02610.x>.
 59. Pracht D, Elm C, Gerber J, Bergmann S, Rohde M, Seiler M, Kim KS, Jenkinson HF, Nau R, Hammerschmidt S. 2005. PavA of *Streptococcus pneumoniae* modulates adherence, invasion, and meningeal inflammation. *Infect Immun* 73:2680–2689. <https://doi.org/10.1128/IAI.73.5.2680-2689.2005>.
 60. Cecchelli R, Aday S, Sevin E, Almeida C, Culot M, Dehouck L, Coisne C, Engelhardt B, Dehouck MP, Ferreira L. 2014. A stable and reproducible human blood-brain barrier model derived from hematopoietic stem cells. *PLoS One* 9:e99733. <https://doi.org/10.1371/journal.pone.0099733>.
 61. Rubens CE, Wessels MR, Heggen LM, Kasper DL. 1987. Transposon mutagenesis of type III group B *Streptococcus*: correlation of capsule expression with virulence. *Proc Natl Acad Sci U S A* 84:7208–7212. <https://doi.org/10.1073/pnas.84.20.7208>.
 62. Hooven TA, Randis TM, Daugherty SC, Narechiana A, Planet PJ, Tettelin H, Ratner AJ. 2014. Complete genome sequence of *Streptococcus agalactiae* CNCTC 10/84, a hypervirulent sequence type 26 strain. *Genome Announc* 2:e01338-14. <https://doi.org/10.1128/genomeA.01338-14>.
 63. Wang NY, Patras KA, Seo HS, Cavaco CK, Rösler B, Neely MN, Sullam PM, Doran KS. 2014. Group B streptococcal serine-rich repeat proteins promote interaction with fibrinogen and vaginal colonization. *J Infect Dis* 210:982–991. <https://doi.org/10.1093/infdis/jiu151>.
 64. Sheen TR, Jimenez A, Wang NY, Banerjee A, van Sorge NM, Doran KS. 2011. Serine-rich repeat proteins and pili promote *Streptococcus agalactiae* colonization of the vaginal tract. *J Bacteriol* 193:6834–6842. <https://doi.org/10.1128/JB.00094-11>.
 65. Austenaa LM, Carlsen H, Hollung K, Blomhoff HK, Blomhoff R. 2009. Retinoic acid dampens LPS-induced NF-kappaB activity: results from human monoblasts and in vivo imaging of NF-kappaB reporter mice. *J Nutr Biochem* 20:726–734. <https://doi.org/10.1016/j.jnutbio.2008.07.002>.
 66. Choi WH, Ji KA, Jeon SB, Yang MS, Kim H, Min KJ, Shong M, Jou I, Joe EH. 2005. Anti-inflammatory roles of retinoic acid in rat brain astrocytes: suppression of interferon-gamma-induced JAK/STAT phosphorylation. *Biochem Biophys Res Commun* 329:125–131. <https://doi.org/10.1016/j.bbrc.2005.01.110>.
 67. Elias KM, Laurence A, Davidson TS, Stephens G, Kanno Y, Shevach EM, O'Shea JJ. 2008. Retinoic acid inhibits Th17 polarization and enhances FoxP3 expression through a Stat-3/Stat-5 independent signaling pathway. *Blood* 111:1013–1020. <https://doi.org/10.1182/blood-2007-06-096438>.
 68. Nozaki Y, Yamagata T, Sugiyama M, Ikoma S, Kinoshita K, Funauchi M. 2006. Anti-inflammatory effect of all-trans-retinoic acid in inflammatory arthritis. *Clin Immunol* 119:272–279. <https://doi.org/10.1016/j.clim.2005.11.012>.
 69. van Neerven S, Nemes A, Imholz P, Regen T, Denecke B, Johann S, Beyer C, Hanisch UK, Mey J. 2010. Inflammatory cytokine release of astrocytes in vitro is reduced by all-trans retinoic acid. *J Neuroimmunol* 229:169–179. <https://doi.org/10.1016/j.jneuroim.2010.08.005>.